

Convert graphene sheets to boron nitride and boron nitride–carbon sheets via a carbon-substitution reaction

Wei-Qiang Han, Hua-Gen Yu, and Zhenxian Liu

Citation: *Appl. Phys. Lett.* **98**, 203112 (2011); doi: 10.1063/1.3593492

View online: <http://dx.doi.org/10.1063/1.3593492>

View Table of Contents: <http://apl.aip.org/resource/1/APPLAB/v98/i20>

Published by the [American Institute of Physics](http://www.aip.org).

Additional information on *Appl. Phys. Lett.*

Journal Homepage: <http://apl.aip.org/>

Journal Information: http://apl.aip.org/about/about_the_journal

Top downloads: http://apl.aip.org/features/most_downloaded

Information for Authors: <http://apl.aip.org/authors>

ADVERTISEMENT

a sampling of our products		for surface and materials science	www. rbdinstruments .com	celebrating over 20 years of innovation
 deposition tools	 desorption systems	 sputter ion sources	 viewports	 usb picoammeters

Convert graphene sheets to boron nitride and boron nitride–carbon sheets via a carbon-substitution reaction

Wei-Qiang Han,^{1,a)} Hua-Gen Yu,² and Zhenxian Liu³

¹Center for Functional Nanomaterials, Brookhaven National Laboratory, Upton, New York 11973, USA

²Department of Chemistry, Brookhaven National Laboratory, Upton, New York 11973, USA

³Geophysical Laboratory, Carnegie Institution of Washington, Washington, DC 20015, USA

(Received 1 April 2011; accepted 2 May 2011; published online 20 May 2011)

Here we discuss our synthesis of highly crystalline pure boron nitride (BN) and BN–carbon (BN–C) sheets by using graphene sheets as templates via a carbon-substitution reaction. Typically, these sheets are several micrometers wide and have a few layers. The composition ratios of BN–C sheets can be controlled by the post-treatment (remove carbon by oxidation) temperature. We also observed pure BN and BN–C nanoribbons. We characterized the BN–C sheets via Raman spectroscopy and density functional theory calculations. The results reveal that BN–C sheets with an armchair C–BN chain, and embedded C₂ or C₆ units in BN-dominated regions energetically are the most favorable. © 2011 American Institute of Physics. [doi:10.1063/1.3593492]

Boron nitride (BN) is a synthetic binary compound located between the III and V group elements in the periodic table. However, its polymorphism and mechanical characteristics are closer to those of carbon compared with other III–V compounds, such as gallium nitride. Such correspondence between BN and carbon readily is understood from their isoelectronic structures.¹ On the other hand, in contrast to graphite, layered BN is transparent and is an insulator. Hitherto, only a few routes have been reported for synthesizing and characterizing BN monolayer or few-layer sheets.^{1–7} Pacilé *et al.*⁴ reported obtaining a two-dimensional h-BN with few atomic layers (more than five layers) employing a micromechanical cleavage method. Han *et al.* generated free-standing monolayer and double-layer BN sheets via a chemical-solution-derived method starting from single-crystalline h-BN.³ Yu *et al.*⁶ prepared BN sheets by a chemical vapor deposition method. Very recently, Ci *et al.*² used a chemical vapor deposition method to produce BN–carbon (BN–C) sheets consisting of randomly distributed domains of h-BN and C phases, with compositions ranging from pure BN to pure graphene. These BN–C sheets might have band gap-engineered applications in electronics and optics, and properties that are distinct from those of graphene and h-BN.

Previously, we developed a method to prepare pure BN and BN–C nanotubes^{8–10} and nanopores¹¹ using carbon nanotubes and active carbon, respectively, as starting templates via a carbon-substitution-reaction method. Metallic single-walled carbon nanotubes have been converted into semiconducting BCN nanotubes by B/N codoping.^{12–14} In the present study, we determined that this same reaction is an efficient route for making BN and BN–C sheets on templates of graphene sheets. We also studied Raman spectra of the BN–C sheets experimentally and theoretically to better understand the chemical bonding of these sheets.

The graphene sheets we used were obtained by a chemical-solution-derived method starting from graphite crystals.^{3,15} The graphite sheets are usually several micrometers wide, and typically the number of layers ranges from a few to 15 layers. We placed B₂O₃ powder in an open graph-

ite crucible, covered it first with some molybdenum oxide as a promoter^{16,17} and then with graphene sheets. The crucible was held in a flowing nitrogen atmosphere at 1650 °C for 30 min. Thereafter, we collected the product was from the bed of graphene sheets. The product was then heated in air at 650 °C (sample A) and 600 °C (sample B), respectively, for 30 min to remove the remaining carbon layers, and some carbon parts from BN–C to obtain pure BN or higher B/C ratio BN–C.¹⁰

Figure 1 is transmission electron microscopy (TEM) images and electron-energy-loss spectroscopy (EELS) spectra taken from sample A. Figure 1(a) is a low-magnification TEM image of several sheets. Figure 1(b) is a high-resolution TEM image of a four-layer sheet. The interplanar spacing of the layers is ~0.34 nm. Figure 1(c) is an EELS spectrum taken from the sheet. The B/N atomic ratio is close to 1, i.e., consistent with a stoichiometry of BN. EELS spectra taken from different sheets show that most of them are pure BN and some of them contain pure BN domains and some BN–C domains with low atomic ratio of C/(B+N+C). Besides sheets, the product contained nanoribbons. Figure 1(d) shows a part of a BN nanoribbon whose width is only about 5 nm.

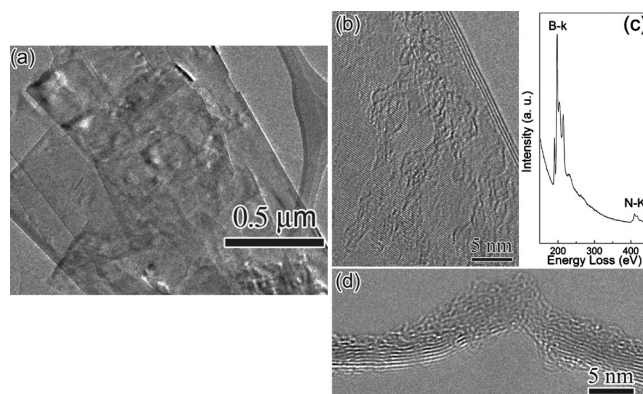


FIG. 1. Sample A (a) low-magnification TEM image of several BN sheets; (b) high-magnification TEM image of a four-layer sheet; (c) an EELS spectrum of the BN sheet; and (d) a BN nanoribbon.

^{a)}Electronic mail: whan@bnl.gov.

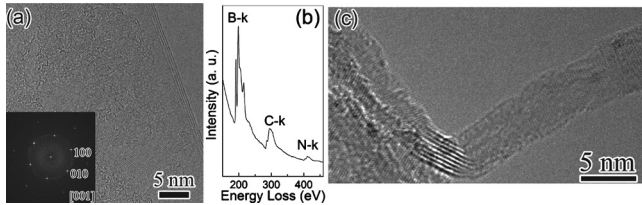
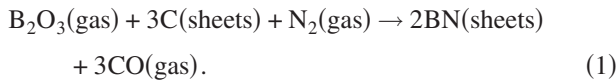


FIG. 2. Sample B (a) high-magnification TEM image of a four-layer BN-C sheet; (b) an EELS spectrum of the BN-C sheet; and (c) a BN-C nanoribbon.

Figure 2 are TEM images and EELS spectra taken from sample B. Figure 2(a) is a high-resolution TEM image of a single-crystalline four-layer sheet along the [001] direction. The inset is an image of the fast-Fourier-transform electron-diffraction patterns that also determine the character of the single crystal. Figure 2(b) is an EELS spectrum taken from the sheet in Fig. 2(b). The C/(B+N+C) atomic ratio is 0.42. The B/N atomic ratio for all spectra is close to 1. Figure 2(c) illustrates a nanoribbon where both sides are smooth; it is folded from the middle, revealing its eight layers. EELS spectrum denoted that it was BN-C with a B/(B+N+C) atomic ratio of 0.28. The B/N atomic ratio is close to 1.

Analogous with the synthesis of BN and BN-C nanotubes and nanopores by the synthesis of carbon-substitution reaction,^{8,11} the synthesis of BN sheets from carbon sheets can be expressed by the following chemical reaction:



When the reaction temperature reaches 1500 °C, the main boron oxide is B₂O₂,¹⁷ which is mainly formed by the reaction of B₂O₃ and CO. The reaction yields small amount of pure BN sheets, and a mix of BN-C ones with high and low B/(B+N+C) atomic ratios. The high reaction temperature makes the produced BN-C sheets still keep high crystallinity. Also present are BN-C sheets with separated BN and carbon layers or domains in the same layer, just like BN-C nanotubes.^{10,18} After oxidation at 600 °C, most BN-C sheets become transformed into high B/C ratio sheets or even pure BN sheets because carbon layers or domains in the BN-C sheets start to undergo oxidation in air at 550 °C while oxidation of the BN layers in air begins only at 800 °C.¹⁰ When the post-treatment temperature is raised to 650 °C, most BN-C sheets become pure BN sheets. This again confirms that BN-C sheet consists of BN and C domains. The holes and nanoribbons usually are formed during oxidation.

Figure 3(a) shows the Raman spectrum of sample A of BN sheets, revealing a clear strong band at 1337 cm⁻¹, and also Raman spectrum for the BN-C sheets of sample B, revealing two strong bands at 1342 and 1572 cm⁻¹. Compared to the weak D (1350 cm⁻¹) and G (1582 cm⁻¹) bands of the graphene sheet,¹⁹ they display noticeable red shifts, which may reflect the C-B and/or C-N chemical bonds in BN-C sheets of sample A rather than physical interactions between the graphene sheets and BN ones.

To clarify this issue of BN-C Raman spectrum, we have used a circumcoronenelike model to mimic single-layer BN-C sheets. Figure 3(b) shows 11 proposed combinations. They have near hexagon symmetry and represent three possible kinds of structures: separated C atoms embedded in a

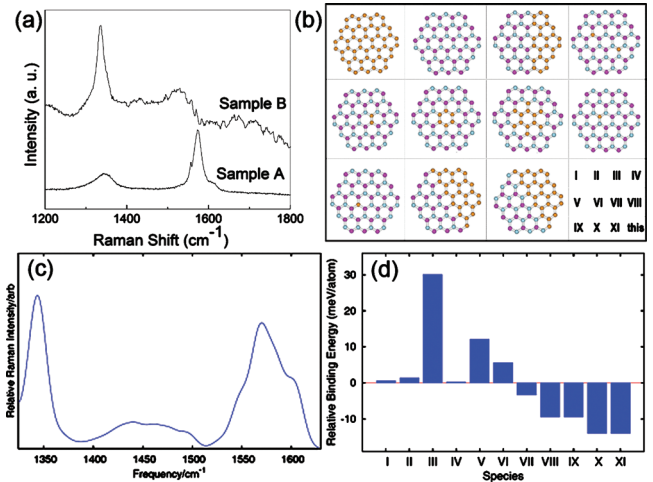


FIG. 3. (Color) (a) Experimental Raman spectra of sample A and sample B; (b) the C (brown), B (purple), and N (blue) skeletons of circumcoronenelike sheets studied in this work, their labeling map is given in the right-bottom panel; (c) simulated Raman spectrum of the armchair-connected BN-C species (III); (d) calculated relative stability of the BN-C sheets among the group in (b).

BN sheet (IV, VIII, and IX); carbon clusters in BN (V-VII); and C-BN linked BN-C sheets (III, X, and XI), in addition to carbon sheets (I) and BN sheets (II) for reference. The geometric optimization and harmonic-frequency analysis of the I-XI BN-C sheets were performed using the hybrid density functional theory (DFT) B3LYP,²⁰ together with the double zeta basis set 6-31G(d).²¹ In the vibrational simulations, Raman spectra were calculated by convoluting the scaled DFT frequencies and intensities with a Gaussian line-shape function of a full width at half maximum of 20 cm⁻¹; this is the approximate line width of BN-C sheets measured experimentally. The scaling factor we used was 0.9547 that is calibrated according to the strongest experimental G band (1582 cm⁻¹) of single layer graphene sheet based on the corresponding theoretical mode of the circumcoronene (I). This factor is very close to the suggested universal one of 0.9614 for the B3LYP/6-31G(d) method.²² The scaling technique largely diminishes the errors due to the size and H-boundary effects in the circumcoronenelike molecular model. Consequently, highly accurate spectra are obtained. All electronic structure calculations were made using the G09 program package.²³

The DFT calculations show that all eleven species are stable and form hexagonal skeletons, consistent Ci *et al.*'s recent observation.² However, those species give different characters of Raman spectra in the 1300–1650 cm⁻¹ range. Although the hydrogen atoms and their edge effect often results more complicated spectra in the simulations, we are able to identify those peculiar features of each species regardless of some weak and/or spurious bands. This is partially due to the fact that the C impurity-related C-N bonds often produce much stronger Raman intensities so that the edge effect fades out. Roughly, the isolated C atom doped B_xN_{x-1}-C sheet (IX) gives a similar Raman spectrum as does a single-layer BN sheet. Predictably, it is a typical 1346 cm⁻¹ band in addition to a strong one at 1406 cm⁻¹. The latter is enhanced by the edge effect. The effect overwhelms the specific E_{2g} mode obtained at 1365.5 cm⁻¹ because a pure BN sheet has rather weak Raman intensities. Since the C impurity introduces only the C-B bonds into the

BN–C sheet (IX), the results may imply that the C–B bonds have a similar Raman intensity contribution as the B–N bonds in BN sheets. Nevertheless, the E_{2g} mode has a strong infrared intensity that can be easily recognized. Compared to the experimental value of 1370 cm^{-1} for h-BN sheets, the theoretical frequency is in excellent agreement within an error of 4.5 cm^{-1} . This just verifies the molecular model used in this work. On the other hand, the isolated C atom doped $B_{x-1}N_x\text{--}C$ produces a new Raman band at 1490 cm^{-1} that is a fingerprint for the formation of C–N bonds in BN–C sheets, such as IV, VIII, and XI. Furthermore, if a C–N zigzag chain is generated, as in XI, the typical Raman band will occur at 1341 cm^{-1} . That is, the persistence of both 1341 and 1490 cm^{-1} Raman peaks are the characteristic features for the zigzag C–N chain in BN–C sheets. Similarly, the characteristic Raman peaks are 1337 and 1534 cm^{-1} for the BN–C sheet X with a zigzag C–B chain. If the zigzag C–B/N chain is embedded within BN sheets, the 1337 cm^{-1} Raman peak will exhibit a blueshift to 1362 cm^{-1} with a band near 1530 cm^{-1} . In particular, the embedded C_2 (V) and benzene C_6 (VI) units will be presented by a unique Raman peak at 1548 cm^{-1} that is smaller than the G band of graphene sheet. Although none of the DFT Raman spectra discussed above match the experimental one in Fig. 3(b), we found that the armchair-linked BN–C sheet (III) produces a similar Raman spectrum as shown in Fig. 3(c). It clearly illustrates two strong peaks at 1344 and 1570 cm^{-1} . The 1570 cm^{-1} band also includes two noticeable shoulders. The agreement between theoretical simulations and experimental results is within 2.0 cm^{-1} . Compared with the G band of a pure carbon sheet, the 1570 cm^{-1} band reveals a big redshift of 12 cm^{-1} . Therefore, this combined experimental and theoretical investigation may well offer a concrete evidence for the chemically bonded BN–C sheet, especially via the C–B/N arm chair connectivity. We were very interested in why the armchair-linked BN–C structure is detected easily. To answer this question, we undertook a statistical analysis within this group of BN–C sheets using the binding-energy (E_b^A) fitting approach,

$$E_b^A = \sum_{\alpha} n_{\alpha} E_{\alpha} - E_A = \sum_{\alpha\beta} n_{\alpha\beta} D_{\alpha\beta} \quad (2)$$

for each species A. Here E_A and E_{α} refer to the DFT energies of molecule A and atom α , respectively. n_{α} is the number of atoms α while $n_{\alpha\beta}$ is the number of the α – β bonds in A. $D_{\alpha\beta}$ are the average bond strengths of the α – β bond in this group of simulated species. They are obtained in electron volt as $D_{CC}=5.785$, $D_{CB}=4.814$, $D_{CN}=4.314$, and $D_{BN}=5.122$, which can be used to determine the relative stability of each species. Figure 3(d) shows our results, where a negative binding energy means a less stable species among the group. Clearly, the most stable BN–C sheet is III with an armchair linked C–B/N structure. In other words, the armchair linked structure is energetically preferable so that there is relatively large fraction in BN–C sheets, or higher Raman intensities. Furthermore, Fig. 3(d) shows that the occurrence of embedded C_2 and benzene C_6 units is likely. This finding does support the experimental observations by Krivanek *et al.*²⁴ and Ci *et al.*² In addition, the weaker C–B and C–N

bond strengths relative to C–C are consistent with the redshift of the Raman peak around 1580 cm^{-1} .

In summary, we prepared BN and BN–C sheets using graphene sheets as templates via a carbon-substitution reaction. We also found BN and BN–C nanoribbons in the product. Expectedly, these sheets will have special physical and chemical properties and great potential for applications in microelectronic, photonic, catalysis, and composite materials.

This research was carried out at the Center for Functional Nanomaterials, Brookhaven National Laboratory (BNL), which is supported by the U.S. Department of Energy, Office of Basic Energy Sciences, under Contract No. DE-AC02-98CH10886. Calculations were performed at NERSC. The use of the U2A beamline for the Raman experiments is supported by COMPRES, the Consortium for Materials Properties Research in Earth Sciences under NSF Cooperative Agreement No. EAR 06-49658.

- ¹W. Q. Han, in *Mixed Metal Nanomaterials*, edited by C. S. S. R. Kumar (Wiley, Weinheim, 2009), p. 411.
- ²L. Ci, L. Song, C. H. Jin, D. Jariwala, D. X. Wu, Y. J. Li, A. Srivastava, Z. F. Wang, K. Storr, L. Balicas, F. Liu, and P. M. Ajayan, *Nature Mater.* **9**, 430 (2010).
- ³W. Q. Han, L. J. Wu, Y. M. Zhu, K. Watanabe, and T. Taniguchi, *Appl. Phys. Lett.* **93**, 223103 (2008).
- ⁴D. Pacilé, J. C. Meyer, Ç. Ö. Girit, and A. Zettl, *Appl. Phys. Lett.* **92**, 133107 (2008).
- ⁵L. Song, L. J. Ci, H. Lu, P. B. Sorokin, C. H. Jin, J. Ni, A. G. Kvashnin, D. G. Kvashnin, J. Lou, B. I. Yakobson, and P. M. Ajayan, *Nano Lett.* **10**, 3209 (2010).
- ⁶J. Yu, L. Qin, Y. F. Hao, S. Kuang, X. D. Bai, Y. M. Chong, W. J. Zhang, and E. Wang, *ACS Nano* **4**, 414 (2010).
- ⁷H. B. Zeng, C. Y. Zhi, Z. H. Zhang, X. L. Wei, X. B. Wang, W. L. Guo, Y. Bando, and D. Golberg, *Nano Lett.* **10**, 5049 (2010).
- ⁸W. Q. Han, Y. Bando, K. Kurashima, and T. Sato, *Appl. Phys. Lett.* **73**, 3085 (1998).
- ⁹W. Q. Han, Y. Bando, K. Kurashima, and T. Sato, *Jpn. J. Appl. Phys., Part 2* **38**, L755 (1999).
- ¹⁰W. Q. Han, W. Mickelson, J. Cumings, and A. Zettl, *Appl. Phys. Lett.* **81**, 1110 (2002).
- ¹¹W. Q. Han, R. Brutchey, T. D. Tilley, and A. Zettl, *Nano Lett.* **4**, 173 (2004).
- ¹²Z. Xu, W. G. Lu, W. L. Wang, C. Z. Gu, K. H. Liu, X. D. Bai, E. G. Wang, and H. J. Dai, *Adv. Mater. (Weinheim, Ger.)* **20**, 3615 (2008).
- ¹³W. L. Wang, X. D. Bai, K. H. Liu, Z. Xu, D. Golberg, Y. Bando, and E. G. Wang, *J. Am. Chem. Soc.* **128**, 6530 (2006).
- ¹⁴W. L. Wang, Y. Bando, C. Y. Zhi, W. Y. Fu, E. G. Wang, and D. Golberg, *J. Am. Chem. Soc.* **130**, 8144 (2008).
- ¹⁵X. L. Li, X. R. Wang, L. Zhang, S. W. Lee, and H. J. Dai, *Science* **319**, 1229 (2008).
- ¹⁶D. Golberg, Y. Bando, K. Kurashima, and T. Sato, *Chem. Phys. Lett.* **323**, 185 (2000).
- ¹⁷W. Q. Han, P. J. Todd, and M. Strongin, *Appl. Phys. Lett.* **89**, 173103 (2006).
- ¹⁸K. Suenaga, C. Colliex, N. Demoncy, A. Loiseau, H. Pascard, and F. Willaime, *Science* **278**, 653 (1997).
- ¹⁹A. C. Ferrari, J. C. Meyer, V. Scardaci, C. Casiraghi, M. Lazzeri, F. Mauri, S. Piscanec, D. Jiang, K. S. Novoselov, S. Roth, and A. K. Geim, *Phys. Rev. Lett.* **97**, 187401 (2006).
- ²⁰C. T. Lee, W. T. Yang, and R. G. Parr, *Phys. Rev. B* **37**, 785 (1988).
- ²¹A. D. McLean and G. S. Chandler, *J. Chem. Phys.* **72**, 5639 (1980).
- ²²A. P. Scott and L. Radom, *J. Phys. Chem.* **100**, 16502 (1996).
- ²³M. J. Frisch, G. W. Trucks, and H. B. Schlegel, in GAUSSIAN 09, Revision A. 1, Gaussian Inc., Wallingford, CT., 2009.
- ²⁴O. L. Krivanek, M. F. Chisholm, V. Nicolosi, T. J. Pennycook, G. J. Corbin, N. Dellby, M. F. Murfitt, C. S. Own, Z. S. Szilagy, M. P. Oxley, S. T. Pantelides, and S. J. Pennycook, *Nature (London)* **464**, 571 (2010).